**High-performance spin filters based on 1,2,4,5-tetrahydroxybenzene molecules attached to bulk nickel electrodes**

Shi Li[1], Yudi Wang[1], Yongfeng Wang[1], Stefano Sanvito[2], Shimin Hou[1*]

1 Key Laboratory for the Physics and Chemistry of Nanodevices, Department of Electronics, Peking University, Beijing 100871, China

2 School of Physics, AMBER and CRANN Institute, Trinity College, Dublin 2, Ireland

ABSTRACT: Achieving highly spin-polarized current at the nanoscale is of paramount importance in molecular spintronics. Using a self-consistent *ab initio* approach that combines the non-equilibrium Green's function formalism with spin density functional theory, we explore the spin transport properties of a set of 1,2,4,5-tetrahydroxybenzene (THB)-based molecular junctions with nickel electrodes. Our calculations show that the junction incorporating a dehydrogenated THB molecule exhibits remarkable spin-filtering effects as well as a high transmission for the spin-down (minority) electrons around the Fermi level. This is due to the favorable alignment of the frontier molecular orbitals relative to the electrode Fermi level and the orthogonality between these π-symmetry molecular states and the 4*s* conducting channels of the nickel electrodes. In addition, the Ni-O bonds at the molecule-electrode interfaces are very robust. The spin-filtering efficiency can be further improved by introducing one more THB molecule and a central nickel atom into the tunneling path. Finally, the adsorption of CO over the central nickel atom significantly promotes the transport of spin-down electrons and reduces that of spin-up (majority) electrons, achieving a nearly 100% spin-polarization at finite bias voltages. Our findings demonstrate the great potentials of these classes of THB-based junctions for future high-performance molecular spintronic devices.

## 1.Introduction

Molecular spintronics, aiming at the active manipulation of both the charge and spin degrees of freedom at the single-molecule level, represents one of the most exciting avenues for building next-generation nanoelectronic devices with high-speed and low-energy consumption capabilities.[1] In particular, organic materials have emerged as promising candidates for spin transport media due to the weak spin-orbit and nuclear hyperfine interactions, which make it feasible to preserve spin-coherence over distances and times much longer than in other materials.[2-3] Moreover, organic molecules have unique functions of chemical selectivity and provide versatility by tuning their electronic and magnetic properties via ligand modifications.[4-6] In this field, one of the core issues concerns the generation of spin-polarized currents composed of electrons of a single spin type. This is the precondition for realizing spintronic devices with a high signal-to-noise ratio. Therefore, spin filters delivering metallic features for one spin channel and insulating for the other have attracted extensive and growing attention.[7-9] An important evaluation criterion for the performance of spin-filter devices is the spin-polarization, defined as $SP = |T_\uparrow - T_\downarrow|/|T_\uparrow + T_\downarrow|$, where $T_\uparrow$ and $T_\downarrow$ represent the transmission coefficients for the spin-up (majority) and spin-down (minority) electrons, respectively. Nowadays, designing spin filters with a large *SP* as well as a high conductance is of considerably fundamental interest and represents a key step towards the development of molecular spintronic devices.

Built with the help of mature break junction techniques, single-molecule junctions that consist of two ferromagnetic electrodes separated by a nonmagnetic spacer have become popular testbeds for the study of spin transport near the limit of spintronics miniaturization. Quite generally, the spin filtering efficiency of a molecular junction is tightly bound up with the electrode materials and the ferromagnetic-organic interfacial properties. As it can be easily shaped at the nanoscale while preserving useful magnetic properties, nickel is widely utilized in many theoretical and experimental investigations as an ideal ferromagnetic electrode material.[10-15] In Ni, although the spin-polarization of the 3*d* electrons is large due to the exchange interaction, that of the 4*s* states is small, resulting in currents with moderate spin polarization. For example, only partially spin-polarized current, with *SP*~ 33%, was reported in Ni nanocontacts due to the fact that 4*s* electrons conduct almost perfectly.[16-18] In order to circumvent

this limitation, Dappe *et al* proposed an *s*-blocking mechanism by joining two ferromagnetic electrodes with a π-conjugated molecule.[19] As a result, the electron transport was mainly associated to the spin-down 3*d* electrons while the 4*s*-conducting channels were fully blocked, leading to an *SP* of 81% at the Fermi level for a Ni-polythiophene-Ni junction. However, a fact that cannot be ignored in such proposed junctions is the presence of a spin-up transmission peak very close to the Fermi level. This means that the spin-filtering efficiency is likely to deteriorate when a finite bias voltage is applied. The feasibility of this symmetry-based mechanism in the design of high-performance spin filters has been widely tested in the past few years.[20-24] Recently, Li *et al*. explored spin-polarized transport across single benzene derivatives attached to nickel electrodes via different anchoring groups.[25] Their calculations show that among all considered molecules the one with nitro (-$NO_2$) terminations preforms best, with a simultaneously high value of *SP* (80%) and conductance (0.36 $G_0$ ). Here $G_0=e^2/h$ is the conductance quantum. However, experiments have uncovered that molecular junctions terminated with nitro anchors break at an inclined angle with respect to the surface normal before being fully extended.[26] Hence, in order to fabricate high-performance, reliable and robust molecular spintronic devices, further studies are highly desirable.

1,2,4,5-tetrahydroxybenzene (THB) is a planar benzene derivative, which can form by self-assembly metal-coordinated networks on metal substrates, indicating unusual conductive, catalytic and magnetic properties.[27-31] Inspired by the aforementioned *s*-blocking mechanism, we investigate the potential of THB molecules to be used as high-performance spin filters when sandwiched between two ferromagnetic nickel electrodes. Combining the non-equilibrium Green's function (NEGF) formalism with density functional theory (DFT) (i.e., the NEGF+DFT approach),[32-38] our calculations show that the spin-polarization at the Fermi level for the Ni-THB-Ni junction is as high as 91%. The low-bias conductance of the spin-down channel is large and no evident peaks are found around the Fermi level in the transmission spectrum for spin-up electrons, resulting in reliable spin-polarization at finite bias voltages. Moreover, the spin filtering efficiency can be further improved by introducing one more THB molecule and a central nickel atom between the electrodes. We also find that the adsorption of small gaseous molecules, such as CO, NO and $NH_3$, on the central nickel atom significantly modifies the junction transport properties. In particular, adsorbing one CO molecule results in nearly 100% spin-polarized electron transport as well as a much larger low-bias conductance.

## 2.Calculation method

In this work, spin-dependent geometry optimization and electronic structure calculations have been performed with the SIESTA package,[39-40] which is an efficient numerical implementation of DFT. We have used the generalized gradient approximation (GGA) within the Perdew-Burke-Ernzerhof (PBE) formulation for the exchange and correlation energy and improved Troullier–Martins norm-conserving pseudopotentials (PPs) to describe the atomic cores.[41-42] The wave functions of the valence electrons are expanded over a finite-range numerical basis set and a user-defined double-zeta plus polarization basis set is constructed for all elements, including hydrogen, carbon, nitrogen, oxygen and nickel. Geometry optimization is performed by standard conjugate gradient until all the atomic forces are less than 0.03 $eV/\dot{A}$. With our choice of PPs and basis set, an optimized lattice constant of 3.56 $\dot{A}$ is obtained for bulk nickel, which is in good agreement with the experimental value of 3.52 $\dot{A}$ and previous DFT calculation value of 3.58 $\dot{A}$.[43] To further confirm the appropriateness of the PPs and the basis functions for nickel, the electronic and magnetic properties of bulk nickel have also been investigated using the VASP code with the same functional.[44] Our SIESTA calculation results agree reasonably well with those obtained with VASP (see Figure S1 in the Supplementary Information - SI).

Spin-polarized transport calculations have been performed using the SMEAGOL code,[45-47] which is a practical implementation of the NEGF+DFT approach. Since SMEAGOL uses SIESTA as the DFT platform, we employ the same PPs, basis sets and GGA functional, for both the geometry relaxation and the transport. The unit cell of the

extended molecule comprises the central molecule, some nickel atoms with low coordination, and ten Ni(111) atomic layers with a 4 × 4 in-plane supercell. The magnetic configurations of these two Ni electrodes are set to be parallel. Here the transport is assumed to be along the *z*-axis, and we always consider periodic boundary conditions in the plane transverse to the transport. An equivalent energy cutoff of 200.0 Ry is taken for the real-space mesh and the Brillouin zone is sampled by 4 × 4 × 1 k-point mesh. The spin-polarized current-voltage (*I-V*) curves of the junction are calculated as

$$I_\sigma = \frac{e}{h}\int_{-\infty}^{+\infty} T_\sigma(V,E)\left[f(E-\mu_L)-f(E-\mu_R)\right]dE, \qquad (1)$$

where $T_\sigma(V,E)$ is the bias-dependent transmission functions for the spin-up and spin-down electrons ($\sigma = \uparrow/\downarrow$), $f(E)$ is the Fermi-Dirac distribution function, and $\mu_{L/R} = E_f \pm eV/2$ is the local Fermi level of the left/right electrode with $E_f$ being the Fermi energy. The transmission functions $T_\sigma(V,E)$ is obtained as

$$T_\sigma(V,E) = Tr[\Gamma_{L,\sigma} G_\sigma^r \Gamma_{R,\sigma} G_\sigma^a](V,E), \qquad (2)$$

where $G_\sigma^{r/a}$ is the retarded (advanced) Green's function of the extended molecule and $\Gamma_{L/R,\sigma}$ is the broadening function matrix describing the interaction of the extended molecule with the left (right)-hand side electrode.

## 3. Results and discussion

We start our studies from the investigation of the spin-polarized electronic transport properties of a THB molecule sandwiched between two bulk nickel electrodes. Figure 1a shows the optimized atomic structure of the Ni-THB-Ni junction. The THB molecule is connected to the two electrodes via a four-atom pyramidal cluster at each side in a symmetric geometry, while a complete dehydrogenation of the four hydroxyl groups is considered. By definition, the dehydrogenated THB molecule was placed in the *y*-*z* plane. Let us stress that the rotation of the central molecule around the *z*-axis has an insignificant impact on the transport properties. In order to find the equilibrium structure, we systematically vary the separation between the two nickel electrodes and optimize the positions of the THB molecule, the nickel atoms in the two pyramidal clusters and those at the

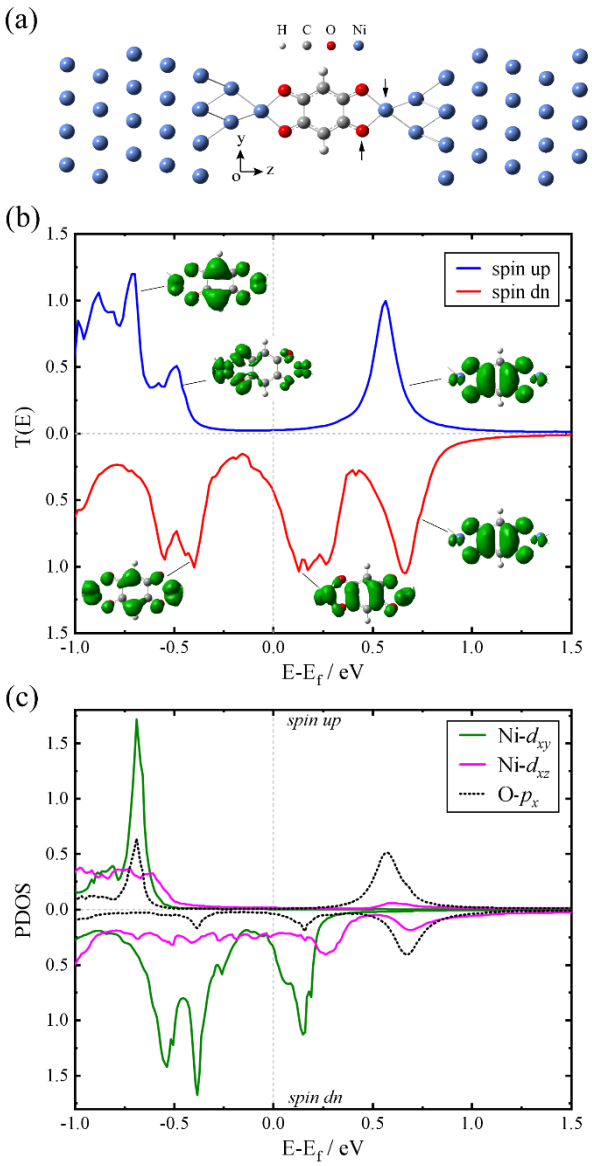


Figure 1. (a) The optimized atomic structure of the Ni-THB-Ni junction; (b) the spin-polarized equilibrium transmission spectra for the spin-up and spin-down electrons, together with the eigenchannels of selected transmission peaks; (c) the PDOS of the $3d_{xy}$ and $3d_{xz}$ orbitals of the Ni apex atom and the $2p_x$ orbital of the O atom [pointed by black arrows in Figure 1a].

electrode surfaces until the total energy reaches a local minimum. The Ni-O bond lengths are optimized to be about 1.97 $\dot{A}$. The corresponding equilibrium transmission function $T_\sigma(E)$ is then calculated and plotted in Figure 1b. For clarity the Fermi level is set to zero, and the blue and red lines are respectively for the spin-up and spin-down transmission

spectra. As we can see, the transmission spectra display remarkably spin-polarized features, with the red curve exceeding the blue one over a broad energy range, going roughly from -0.60 eV to 0.50 eV. Clearly all the prominent transmission peaks for the spin-up electrons lie far away from $E_f$ and decay rapidly towards it, resulting in a tiny low-bias majority-spin conductance. On the contrary, for the spin-down electrons, there is one significantly broad and high transmission peak located at around 0.20 eV, whose tail extends below $E_f$ and provides a much higher transmission at $E_f$. In order to quantify the remarkable difference in transmission of the two spin channels, $T_\uparrow(E_f)$ and $T_\downarrow(E_f)$ are respectively calculated to be 0.024 and 0.47, and the corresponding spin-polarization is obtained as 91%. As a result, the Ni-THB-Ni junction exhibits excellent spin-filtering effects as well as a large equilibrium transmission around the Fermi level. In addition, one more important issue we want to address here concerns the strength of the electrode-molecule bond, which is crucial for the formation of practical molecular junctions. The Ni-O bonding energy in the Ni-THB-Ni junction is evaluated to be -1.64 eV, suggesting a stable interface coupling. Here, the bonding energy is defined as $(E_{jun}-E_{Ni}-E_{mol}+2E_{H_2})/4$, where $E_{jun}$, $E_{Ni}$, $E_{mol}$ and $E_{H_2}$ denote the total energy of the Ni-THB-Ni junction, the bare nickel electrodes, the isolated THB molecule, and the isolated hydrogen molecule, respectively; the unit cells of these subsystems are kept the same as that of the junction. In reference [25] spin-polarized transport across a single benzene derivative attached to the Ni(111) electrodes with the nitro groups was suggested. However, in that case, the Ni-O bonding energy was only -0.91 eV [calculated as $(E_{jun}-E_{Ni}-E_{mol})/4$]. Therefore, when compared to previous studies, the junctions constructed with THB molecules investigated here appear more promising for the fabrication of high-performance, reliable and robust molecular spintronic devices.

Next, we move to reveal the origin of the dramatically different transport properties of the two spin channels. The conductance of a molecular junction is determined by two fundamental factors: firstly, the alignment of the frontier molecular orbitals (FMOs) relative to the Fermi level of the electrodes, and secondly the coupling between the FMOs and the electronic states of the electrodes. Here, we briefly introduce the electronic properties of the isolated THB molecule as a prequel to the analysis of the junction transport. In Figure S2a of the SI we show the FMOs of THB in the gas phase. When the THB molecule is placed in the *y*-*z* plane, the LUMO+1, LUMO, HOMO, and HOMO-1 are dominated by the $2p_x$ atomic orbitals of carbon and oxygen; in contrast, the hydrogen atoms of the hydroxyl groups provide a minor contribution. Here, HOMO and LUMO are respectively the acronyms for the highest occupied molecular orbital and the lowest unoccupied molecular orbital. Different from these $\pi$-type orbitals, the HOMO-2 and HOMO-3 states are both $\sigma$-type, mainly composed of the $2p_y$ and $2p_z$ atomic orbitals of carbon and oxygen.

In order to provide an intuitive understanding of the coupling between the FMOs and the electrode states, the transmission eigenchannels[48-49] for selected resonance peaks are calculated and depicted in Figure 1b. From these we can visually determine the dominating molecular orbitals responsible for the electron transport. Clearly, for spin-up electrons, the transmission peaks centered at 0.56 eV, -0.50 eV and -0.70 eV are dominated by the HOMO, HOMO-3 and HOMO-1 of THB, respectively. As for the spin-down electrons, the transmission peaks above $E_f$ originate completely from the HOMO, while the dual-peak structure around -0.50 eV can be ascribed to the HOMO-1. Taken all together, we confirm that the junction transport properties around $E_f$ are mainly determined by the THB HOMO and HOMO-1. Since the hydroxyl groups are assumed to undergo complete dehydrogenation when connected to nickel apexes, the central molecule will lose four electrons. At the same time, charge transfer also happens between the electrodes and the central molecule due to the different electronegativity of nickel and oxygen. The overall effect is that the original THB HOMO is found unoccupied and located above $E_f$. We now turn our attention to the apex nickel atoms at the electrode-molecule interfaces. According to the Mulliken population analysis, the magnetic moment of the nickel apex atoms is predicted to be roughly 1.0 $\mu_B$, significantly larger than that obtained for bulk ($\approx 0.6\,\mu_B$) and surface ($\approx 0.7\,\mu_B$) nickel

atoms. This enhancement can be understood from the exchange splitting of $3d$ orbitals, which is increased by the lower coordination of the Ni apex atoms and by the bonding to O (the magnetic moment of NiO is approximately $2\,\mu_B$).[50-52] The magnetic moment of the Ni apexes is mainly contributed by the highly spin-polarized $3d$ states but not from the 4*s* ones, since the projected density of states (PDOS) for the latter are found comparable for the two spin channels (see Figure S4). As we have discussed above, the molecular orbitals dominating transport are both of $\pi$-symmetry, edged with the O $2p_x$ atomic orbitals. These would definitely have zero overlap with the 4*s* orbitals of the Ni apexes since the 4*s* and $2p_x$ orbitals do not share the same angular momentum about the bond axis. Hence, in an ideal bonding geometry, injecting spin-unpolarized 4*s* electrons in both spin channels would be completely blocked at the molecule-electrode interface. In contrast, the $\pi$-type HOMO and HOMO-1 states can strongly interact with the $3d$ orbitals of the Ni apexes. More specifically, the THB HOMO, where the O atoms at the ortho-positions have the same orbital phase, interacts with the $3d_{xy}$ and $3d_{xz}$ states of Ni apex, as shown in Figure 1c. Furthermore, the HOMO-1 state, where the O atoms at the ortho-positions have the reverse orbital phases, selectively couples with $3d_{xy}$ ones. It should be noted that the σ-type HOMO-3 orbital interacts strongly with the $3d_{yz}$ state of the Ni apex contributing to the transmission peak at -0.51 eV for the spin-up channel. Based on the above analysis, the origin of the pronounced spin-polarized transport properties can now be summarized as follows: (1) the nickel electrodes could provide highly spin-polarized incoming *d* electrons through the apex atoms of the pyramidal clusters, which is an essential prerequisite; (2) the $\pi$-type frontier molecular orbitals play a leading role for the transport around the Fermi level, since they primarily interact with the $3d_{xy}$ and $3d_{xz}$ states of the apex Ni atoms but are orthogonal to the spin-unpolarized 4*s* states; (3) the resonance peaks for spin-up electrons are located far away from the Fermi level.

Now we investigate the spin-filtering effciency of the Ni-THB-Ni junction at finite bias voltages, which is calculated up to 0.5 V with an interval of 0.1 V. Figure 2 shows the bias-dependent transmission spectra and the spin-polarized electric currents. We observe that the applied bias voltages only modify the transmission around the Fermi level slightly for the spin-up electrons. In contrast, the transmission function for the spin-down electrons changes substantially following the increase of the applied bias while maintaining high values for the transmission coefficients within the bias window. As a result, highly spin-polarized currents are obtained at finite bias voltages; for instance, $I_\downarrow$ is 5.7 μA at 0.3 V, roughly 19 times larger than $I_\uparrow$ (0.3 μA).

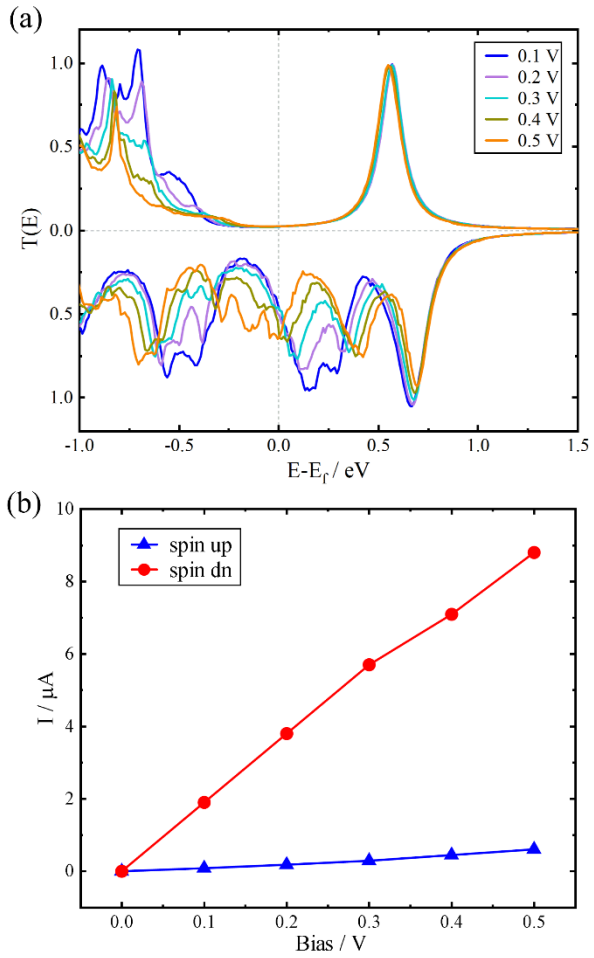


Figure 2. The bias-dependent transmission spectra (a) and the corresponding spin-polarized I-V curves (b) of the Ni-THB-Ni junction calculated from 0.1 V to 0.5 V

A deeper insight into the *s*-forbidden mechanism can be obtained by comparing our results with calculations of a nickel nanocontact without the THB molecule. This model is simply formed by connecting the two electrodes directly through the pyramidal clusters, as depicted in Figure S3 (see

SI). The transmission coefficient at $E_f$ is obtained as 3.4, of which 1.1 comes from the spin-up channel and 2.3 from the spin-down one, leading to a spin-polarization of only 35%. The PDOS spectra of the atomic orbitals of the Ni apexes show similar features to that of the Ni-THB-Ni junction. Nevertheless, in this nanocontact the 4*s* and $3d_{z^2}$ orbitals of one Ni apex can overlap with those of the opposite one, forming an open conducting channel for both spin-up and spin-down electrons (see details in SI). In other words, the unpolarized 4*s* electrons are able to contribute to the junction transport equally for both spins. Hence, despite the fewer *d* states around the Fermi level compared with those of the spin-down channel, the spin-up conductance is still considerable and thus the spin-filtering effect of the nickel nanocontact is poor.

As we have illustrated, the injection of 4*s* states may be completely blocked at the electrode-molecule interface, due to the orthogonality of the 4*s* orbital of Ni apex atoms and the O $2p_x$ atomic orbital, as schematically shown in Figure S6a. However, realistic molecular junctions may deviate from this ideal situation. For example, if the Ni-O bond axis is not strictly aligned in the THB molecule plane, the 4*s* electrons could leak out and decrease the spin filtering efficiency [see Figure S5b-c in the SI]. A straightforward strategy to make up for such loss is to introduce additional *s*-forbidden interfaces along the transport channel. Based on this assumption, we construct the junction model displayed in Figure 3a, where one more dehydrogenated THB molecule and a central nickel atom (pointed by a black arrow) are included, while the rest of the electrode-molecule interface remains unchanged. As expected, $T_\uparrow(E_f)$ and $T_\downarrow(E_f)$ are respectively calculated to be $3.6\times10^{-3}$ and 0.14, resulting in an improved spin-polarization of 95%. The corresponding transmission spectra are shown in Figure 3b. As we can see, in the interval [-0.50, 0.25] eV there are absolutely no peaks appearing for the spin-up electrons and the transmission is negligible. Compared to that of the Ni-THB-Ni junction, the transmission coefficients around $E_f$ now drop for both the spin-up and spin-down channels. One apparent reason for this change is the exponential decay of the tunneling probability with increasing the tunneling barrier length.[53] As a matter of

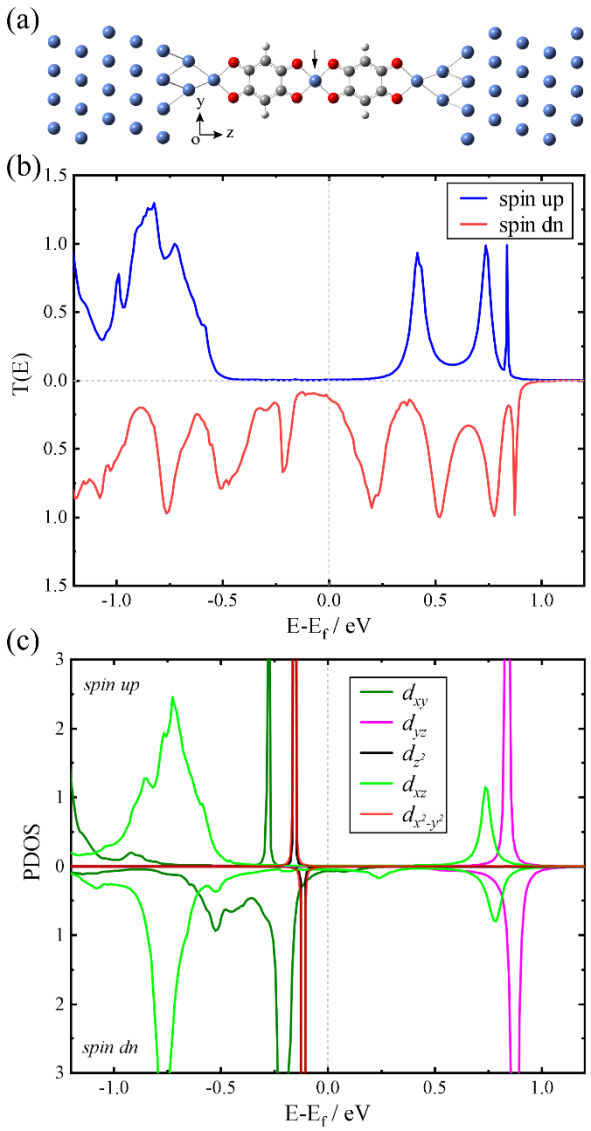


Figure 3. (a) The optimized atomic structure of the Ni-THB-Ni-THB-Ni junction, (b) the spin-polarized equilibrium transmission spectra for the spin-up and spin-down electrons, (c) the PDOS of the 3*d* orbitals of the central Ni atom [pointed by black arrow in (a)].

fact, what we mostly concern is whether the injecting 4*s* electrons are effectively blocked when flowing across the central molecule. Inspection of the FMOs of THB-Ni-THB [see Figure S2b in the SI] suggests that these are composed of two kinds of orbitals, namely the molecular orbitals of THB and the Ni $3d$ atomic orbitals, while the Ni 4*s* states are not involved. Notably, the magnetic moment of the central nickel

atom is zero in both the isolated THB-Ni-THB molecule and the Ni-THB-Ni-THB-Ni molecular junction. The PDOS spectra of the central nickel atom demonstrate that the transmission peaks around $E_f$ for spin-down electrons are associated with the $3d_{xy}$ and $3d_{xz}$ orbitals, as shown in Figure 3c. Other $3d$ orbitals appear as narrow peaks ($3d_{z^2}$, $3d_{x^2-y^2}$) or located far away from $E_f$ ($3d_{yz}$), thus make little contribution to the transport around $E_f$. More importantly, the $4s$ orbitals show a negligible value near $E_f$, an order of magnitude lower than that of the Ni apex. Therefore, we believe that when tunneling occurs through the central molecule, the $4s$ electrons could also be filtered, thus further promote the spin-filtering efficiency. Moreover, the high spin-filtering efficiency is retained when a finite bias voltage is applied across the junction or a moderate change occurs to the junction geometry [see Figures S6 and S7].

The introduction of the central Ni atom in the Ni-THB-Ni-THB-Ni junction not only enhances the spin-filtering effects but also provides additional possibility of controlling the spin transport properties via an external stimulus. Recently, many experimental and theoretical studies have demonstrated that chemical adsorption of small molecules offers an efficient tool to manipulate the transport properties of single-molecule junctions.[54-56] Considering the unsaturated coordination of the central Ni atom, we expect that adsorption of small gaseous molecules like CO, NO and $NH_3$ could alter the electronic and magnetic properties of the central molecule and thus further tune the junction transport. Herein, we first discuss the ligand effects on the atomic and electronic structures of the isolated THB-Ni-THB molecule, with Figure 4a-c showing the most stable adsorption configurations. The key adsorption parameters, namely the adsorption distances, the Ni-O bond lengths, and the adsorption energies are summarized in Table 1. Structural relaxation demonstrates that the central Ni atom forms an axial coordination bond with the carbon atom of CO in a linear binding geometry. In contrast, NO prefers to be stabilized in a bent conformation ($\angle \mathrm{Ni-N-O} = 122.95°$). The adsorption distances from the central Ni atom to CO, NO and $NH_3$ are optimized to be 1.82 $\dot{A}$, 1.80 $\dot{A}$ and 2.17 $\dot{A}$, respectively. In the cases of CO and NO adsorption, the central Ni atom is dragged out of the

Table 1. Adsorption parameters including the adsorption distance ($H$), the Ni-O bond length ($L$), the adsorption energy ($E_{ads}$), and the magnetic moment ($M$) of the central Ni atom.

| | Pristine | CO | NO | $NH_3$ |
|---|---|---|---|---|
| $H/\dot{A}$ | | 1.82 | 1.80 | 2.17 |
| $L/\dot{A}$ | 1.85 | 2.04 | 2.04 | 1.90 |
| $E_{ads}/eV$ | | -0.98 | -1.00 | -0.59 |
| $M/\mu_B$ | 0 | 1.04 | 0.91 | 0.57 |

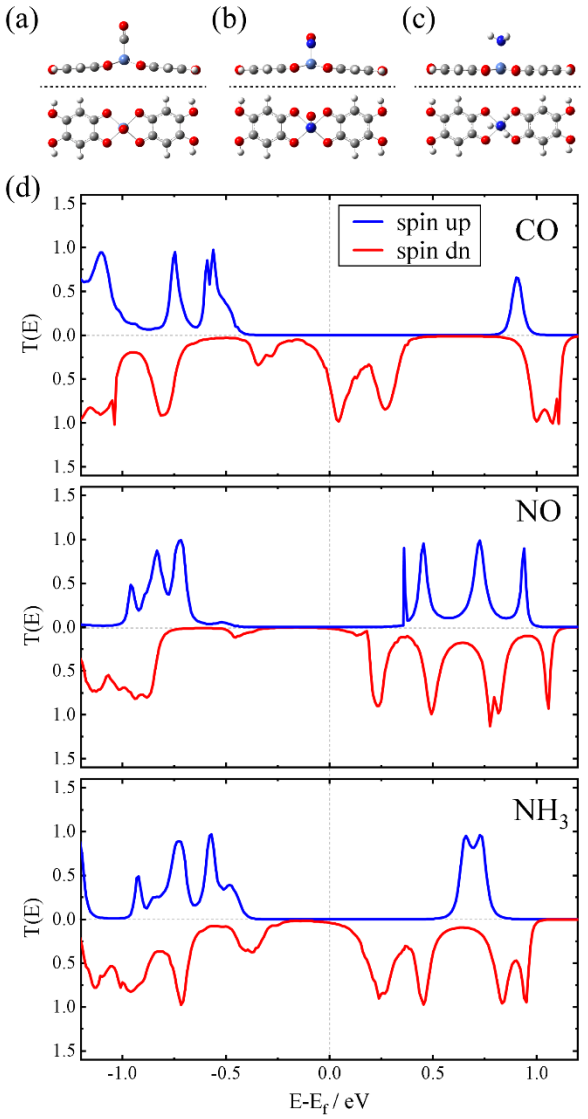


Figure 4. Side views and top views of the optimized atomic structures of the isolated THB-Ni-THB molecule adsorbed with CO (a), NO (b), and $NH_3$ (c) on the central Ni atom, and the spin-polarized equilibrium transmission spectra (d) of the gas-adsorbed Ni-THB-Ni-THB-Ni molecular junctions.

original molecular plane distinctly, whereas for $NH_3$ it remains in plane. The out-of-plane shift of the Ni atom also reduces the in-plane interaction, with the Ni-O bond lengths stretched to different extent. For a quantitative description of the gas adsorption strength, we calculate the adsorption energy $E_{ads}$ that is defined as $E_{ads} = E_{mol+gas} - E_{mol} - E_{gas}$, where $E_{mol+gas}$, $E_{mol}$, and $E_{gas}$ denote the total energy of the gas-adsorbed THB-Ni-THB molecule, the pristine THB-Ni-THB molecule, and the isolated gas molecule, respectively. As listed in Table 1, NO has the most negative adsorption energy (-1.00 eV), comparable to that of CO (-0.98 eV), while $NH_3$ has the weakest adsorption strength (-0.59 eV). This reveals that all these adsorption configurations are energetically favorable. Notably, the adsorption of CO, NO and $NH_3$ induces a significant magnetic moment at the central Ni atom (see Table 1). More details about the electronic and magnetic properties of the gas-adsorbed THB-Ni-THB molecules can be found in the SI (see Figures S2c-S2e).

Finally, we investigate how the electron transport gets modified with the gas adsorption when THB-Ni-THB is sandwiched between the two nickel electrodes. The optimized atomic structures of Ni-THB-Ni-THB-Ni junctions adsorbed with gas molecules are presented in Figure S8. The spin-polarized transmission spectra, displayed in Figure 4d, prove that gas adsorptions considerably alter the junction transport properties. For CO adsorption, a prominent dual-peak structure appears slightly above $E_f$ for spin-down electrons, leading to a transmission coefficient of 0.61 at $E_f$, roughly 3 times larger than that of the pristine junction (0.14). In contrast, the transmission coefficients for spin-up electrons are negligible in the energy interval [-0.40, 0.70] eV; for example, it is 8.0 x $10^{-5}$ at $E_f$. CO adsorption results in a nearly perfect spin-filtering with a spin-polarization value approaching 100%. Our calculations suggest that the CO-adsorbed Ni-THB-Ni-THB-Ni junction is able to generate fully spin-polarized currents at finite bias voltages. Upon NO adsorption, the transport of spin-down electrons around $E_f$ are hugely inhibited. Clearly, the transmission coefficients are very small over a broad energy window around $E_f$ for both spin channels, indicating a poor low-bias conductance as well

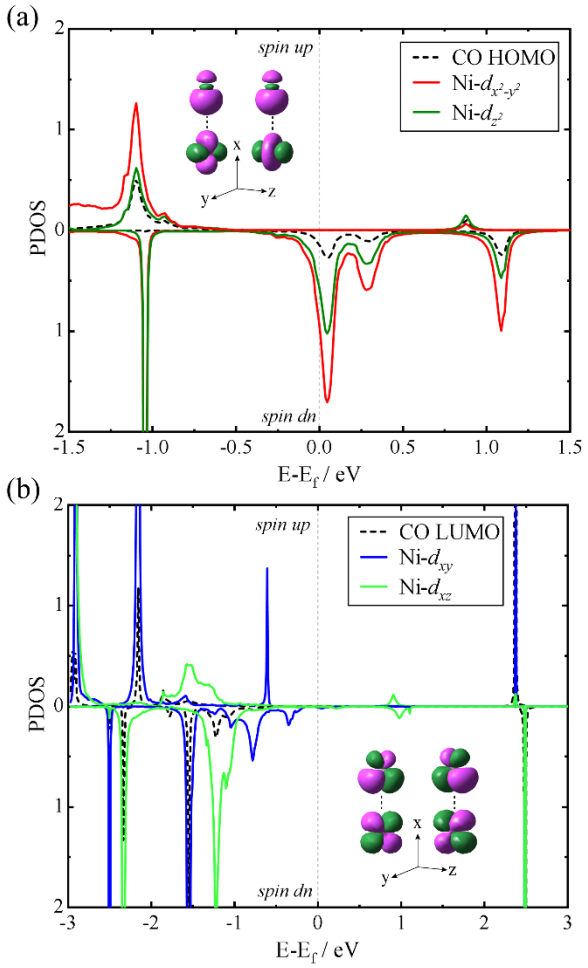


Figure 5. (a) The PDOS of the CO HOMO and the $3d_{z^2}$ and $3d_{x^2-y^2}$ orbitals of the central nickel atom, (b) the PDOS of the CO LUMO and the $3d_{xy}$ and $3d_{xz}$ orbitals of the central nickel atom. The inserts are provided to demonstrate the right symmetry between the CO HOMO/LUMO and the corresponding 3d orbitals of the central Ni atom, but are not intended to show their bonding or anti-bonding nature.

as a poor spin-filtering efficiency. $NH_3$ adsorption only introduces moderate changes to the electron transport as compared to those of CO and NO ligands. The reason can be related to the fact that $NH_3$ has a much weaker adsorption strength than the latter two, so that it modifies only marginally the electronic structure of the junction. It has been widely accepted that the metal-ligand bonding interaction can be described by two components. The first component is the charge donation from the ligand's lone pair into empty metal *d* orbitals. This electron donation makes the metal atom more

electron rich, and thus filled *d* orbitals may interact with the empty orbitals of the ligand to relieve the increased electron density. This is called back-donation (the second component). In the following section, we demonstrate that the abovementioned remarkable changes of the transport properties induced by the adsorption of gas molecules can be associated to the metal-ligand bonding interaction.

Please note that the ligand CO is along the *x*-axis, perpendicular to the THB plane. In this situation, only the $3d_{z^2}$ and $3d_{x^2-y^2}$ orbitals of the central Ni atom have the right symmetry to interact with the CO HOMO, which is primarily derived from the C $2p_x$ orbital. In the pristine Ni-THB-Ni-THB-Ni junction, the $3d_{z^2}$ and $3d_{x^2-y^2}$ orbitals of the central Ni atom appear as narrow peaks in the PDOS spectra below $E_f$ [see Figure 3c]. This indicates that such states are fully occupied and highly decoupled from the two THB molecules. With the CO ligand approaching, electrons are repelled and removed from the $3d_{z^2}$ and $3d_{x^2-y^2}$ states in order to make room for the electron donation from the carbon atom, in other words, from the CO HOMO. As a consequence, the sharp PDOS peaks are found markedly broadened and shifted upwards after CO adsorption, as displayed in Figure 5a. The PDOS curves show the same qualitative shape for the CO HOMO and the Ni $3d_{z^2}$ / $3d_{x^2-y^2}$ atomic orbitals, further confirming the intimate interaction between them. Moreover, the adsorption of CO brings distinct influences to spin-up and spin-down electrons and makes the $3d_{z^2}/3d_{x^2-y^2}$ states spin-polarized. Due to the non-coplanar configuration of the CO-adsorbed THB-Ni-THB molecule, the $3d_{z^2}/3d_{x^2-y^2}$ orbitals of the central nickel atom can now overlap with the π-type orbitals of THB. As we can see, the significant PDOS peaks centered at 0.05 eV and 0.27 eV for the spin-down channel are in good agreement with the locations of the transmission peaks [see Figure 4d]. In contrast, the values of PDOS for the spin-up channel are extremely small around $E_f$. Furthermore, the back-donation of electrons from the central Ni atom to the CO ligand is also found, although it makes minor contributions to the transmission around $E_f$. By symmetry, the Ni $3d_{xy}$ and $3d_{xz}$ atomic orbitals are able to overlap with the doubly degenerate π-type LUMO of CO. The PDOS spectra in Figure 5b suggest that the $3d_{xy}$ and $3d_{xz}$ orbitals of the central Ni atom share some electrons with the CO LUMO, making the latter partially occupied. Clearly the boost of the low-bias transport upon CO adsorption for spin-down electrons is a direct consequence of the redistribution of the $3d_{z^2}/3d_{x^2-y^2}$ electrons of the central Ni atom.

Despite the fact that the NO HOMOs are π-type and σ-type respectively for spin-up and spin-down electrons, they both donate electrons to the Ni $3d_{z^2}$ and $3d_{x^2-y^2}$ atomic orbitals due to the bent ligand bonding, as shown in Figure S9a of the SI. For the spin-up channel, the NO LUMO is degenerate in energy with the HOMO and overlaps with the Ni $3d_{xz}$ orbital forming $d_\pi - p_\pi^*$ back-bonding molecular states [Figure S9b of the SI]. As for the spin-down channel, the degenerate LUMOs are both π-type, one of which overlaps with the Ni $3d_{xz}$ orbital [Figure S9b], while the other with the Ni $3d_{z^2}$ and $3d_{x^2-y^2}$ orbitals [Figure S9c]. The PDOS values of the Ni 3*d* orbitals are very small around the Fermi level, resulting in a much lower transmission. Turning to the $NH_3$ adsorption, the $NH_3$ HOMO interacts with the Ni $3d_{z^2}$ and $3d_{x^2-y^2}$ orbitals [see Figure S9d], similarly to the cases of CO and NO adsorption. However, the back-donation is almost absent, a fact that should be at the root of the lower adsorption strength.

## 4.Conclusion

By employing the NEGF+DFT approach, we have investigated the spin-polarized transport properties of a set of THB-based single-molecule junctions with bulk nickel electrodes, which show great potentials as high-performance and structurally reliable spin filters. When THB is connected to the nickel electrodes via pyramidal clusters, the dominating molecular orbitals for transport are π-type. Hence, they strongly interact with the $3d_{xy}$ and $3d_{xz}$ states of Ni apex atoms but have zero overlap with the 4*s* states, contributing to high spin-filtering effects as well as a large conductance of the spin-down channel. The favorable alignment of these π-type molecular orbitals makes the transmission peaks for spin-up electrons locate far away from the Fermi level, demonstrating that the Ni-THB-Ni junction will act as a good spin filter even at finite bias voltages. The spin-filtering efficiency is promoted in the Ni-THB-Ni-THB-Ni junction,

in which the 4$s$ electrons can be further blocked when crossing the central nickel atom. Furthermore, the adsorption of ligand gas molecules such as CO, NO, and $NH_3$ on the central nickel atom significantly modifies the junction transport properties. In particular, the adsorption of one CO molecule induces a nearly 100% spin-polarized transport. This can be attributed to the redistribution of $3d_{z^2}/3d_{x^2-y^2}$ electrons of the central nickel atom. Our findings can be extended to the design of molecular spintronic devices with other ferromagnetic electrodes like Fe and Co.

**ACKNOWLEDGMENT**

This project was supported by the National Natural Science Foundation of China (Grant No. 21933002), the National Key Research & Development Program (Grant Nos. 2016YFA0201901 and 2018YFA0306003) and High-performance Computing Platform of Peking University. SS thanks Science Foundation Ireland (AMBER Center grant 12/RC/2278_P2) for financial support.

* The corresponding author. E-mail: smhou@pku.edu.cn

## References

1. Sanvito, S., Molecular Spintronics. *Chemical Society Reviews* **2011**, *40*, 3336-3355.

2. Tsurumi, J.; Matsui, H.; Kubo, T.; Hausermann, R.; Mitsui, C.; Okamoto, T.; Watanabe, S.; Takeya, J., Coexistence of Ultra-Long Spin Relaxation Time and Coherent Charge Transport in Organic Single-Crystal Semiconductors. *Nature Physics* **2017**, *13*, 994-999.

3. Dediu, V. A.; Hueso, L. E.; Bergenti, I.; Taliani, C., Spin Routes in Organic Semiconductors. *Nature Materials* **2009**, *8*, 707-716.

4. Coronado, E.; Yamashita, M., Molecular Spintronics: The Role of Coordination Chemistry. *Dalton Transactions* **2016**, *45*, 16553-16555.

5. Venkataramani, S.; Jana, U.; Dommaschk, M.; Soennichsen, F. D.; Tuczek, F.; Herges, R., Magnetic Bistability of Molecules in Homogeneous Solution at Room Temperature. *Science* **2011**, *331*, 445-448.

6. Strozecka, A.; Soriano, M.; Pascual, J. I.; Palacios, J. J., Reversible Change of the Spin State in a Manganese Phthalocyanine by Coordination of Co Molecule. *Physical Review Letters* **2012**, *109*, 147202.

7. Sen, S.; Chakrabarti, S., Ferromagnetically Coupled Cobalt-Benzene-Cobalt: The Smallest Molecular Spin Filter with Unprecedented Spin Injection Coefficient. *Journal of the American Chemical Society* **2010**, *132*, 15334-15339.

8. Requist, R.; Baruselli, P. P.; Smogunov, A.; Fabrizio, M.; Modesti, S.; Tosatti, E., Metallic, Magnetic and Molecular Nanocontacts. *Nature Nanotechnology* **2016**, *11*, 499-508.

9. Herrmann, C.; Solomon, G. C.; Ratner, M. A., Organic Radicals as Spin Filters. *Journal of the American Chemical Society* **2010**, *132*, 3682-3684.

10. Aragones, A. C.; Aravena, D.; Cerda, J. I.; Acis-Castillo, Z.; Li, H.; Antonio Real, J.; Sanz, F.; Hihath, J.; Ruiz, E.; Diez-Perez, I., Large Conductance Switching in a Single-Molecule Device through Room Temperature Spin-Dependent Transport. *Nano Letters* **2016**, *16*, 218-226.

11. Lee, S. K.; Ohto, T.; Yamada, R.; Tada, H., Thermopower of Benzenedithiol and C-60 Molecular Junctions with Ni and Au Electrodes. *Nano Letters* **2014**, *14*, 5276-5280.

12. Brooke, R. J.; Jin, C.; Szumski, D. S.; Nichols, R. J.; Mao, B.-W.; Thygesen, K. S.; Schwarzacher, W., Single-Molecule Electrochemical Transistor Utilizing a Nickel-Pyridyl Spinterface. *Nano Letters* **2015**, *15*, 275-280.

13. Caliskan, S.; Laref, A., The Anchoring Effect on the Spin Transport Properties and I-V Characteristics of Pentacene Molecular Devices Suspended between Nickel Electrodes. *Physical Chemistry Chemical Physics* **2014**, *16*, 13191-13208.

14. Petta, J. R.; Slater, S. K.; Ralph, D. C., Spin-Dependent Transport in Molecular Tunnel Junctions. *Physical Review Letters* **2004**, *93*, 136601.

15. Waldron, D.; Haney, P.; Larade, B.; MacDonald, A.; Guo, H., Nonlinear Spin Current and Magnetoresistance of Molecular Tunnel Junctions. *Physical Review Letters* **2006**, *96*, 166804.

16. Jacob, D.; Fernandez-Rossier, J.; Palacios, J. J., Magnetic and Orbital Blocking in Ni Nanocontacts. *Physical Review B* **2005**, *71*, 220403.

17. Smogunov, A.; Dal Corso, A.; Tosatti, E., Ballistic Conductance and Magnetism in Short Tip Suspended Ni Nanowires. *Physical Review B* **2006**, *73*, 075418.

18. Haefner, M.; Viljas, K.; Frustaglia, D.; Pauly, F.; Dreher, M.;

Nielaba, P.; Cuevas, J. C., Theoretical Study of the Conductance of Ferromagnetic Atomic-Sized Contacts. *Physical Review B* **2008**, *77*, 104409.

19. Smogunov, A.; Dappe, Y. J., Symmetry-Derived Half-Metallicity in Atomic and Molecular Junctions. *Nano Letters* **2015**, *15*, 3552-3556.

20. Vardimon, R.; Klionsky, M.; Tal, O., Indication of Complete Spin Filtering in Atomic-Scale Nickel Oxide. *Nano Letters* **2015**, *15*, 3894-3898.

21. Li, D.; Dappe, Y. J.; Smogunov, A., Perfect Spin Filtering by Symmetry in Molecular Junctions. *Physical Review B* **2016**, *93*, 201403.

22. Rakhmilevitch, D.; Sarkar, S.; Bitton, O.; Kronik, L.; Tal, O., Enhanced Magnetoresistance in Molecular Junctions by Geometrical Optimization of Spin-Selective Orbital Hybridization. *Nano Letters* **2016**, *16*, 1741-1745.

23. Li, D.; Banerjee, R.; Mondal, S.; Maliyov, I.; Romanova, M.; Dappe, Y. J.; Smogunov, A., Symmetry Aspects of Spin Filtering in Molecular Junctions: Hybridization and Quantum Interference Effects. *Physical Review B* **2019**, *99*, 115403.

24. Li, D., Highly Conductive and Complete Spin Filtering of Nickel Atomic Contacts in a Nitrogen Atmosphere. *Physical Review B* **2019**, *99*, 174438.

25. Li, D.; Dappe, Y. J.; Smogunov, A., Tuning Spin Filtering by Anchoring Groups in Benzene Derivative Molecular Junctions. *Journal of Physics-Condensed Matter* **2019**, *31*, 405301.

26. Gulcur, M.; Moreno-Garcia, P.; Zhao, X.; Baghernejad, M.; Batsanov, A. S.; Hong, W.; Bryce, M. R.; Wandlowski, T., The Synthesis of Functionalised Diaryltetraynes and Their Transport Properties in Single-Molecule Junctions. *Chemistry-a European Journal* **2014**, *20*, 4653-4660.

27. Bebensee, F.; Svane, K.; Bombis, C.; Masini, F.; Klyatskaya, S.; Besenbacher, F.; Ruben, M.; Hammer, B.; Linderoth, T., Adsorption and Dehydrogenation of Tetrahydroxybenzene on Cu(111). *Chemical Communications* **2013**, *49*, 9308-9310.

28. Bebensee, F.; Svane, K.; Bombis, C.; Masini, F.; Klyatskaya, S.; Besenbacher, F.; Ruben, M.; Hammer, B.; Linderoth, T. R., A Surface Coordination Network Based on Copper Adatom Trimers. *Angewandte Chemie-International Edition* **2014**, *53*, 12955-12959.

29. Svane, K. L.; Linderoth, T. R.; Hammer, B., Structure and Role of Metal Clusters in a Metal-Organic Coordination Network Determined by Density Functional Theory. *Journal of Chemical Physics* **2016**, *144*, 084708.

30. Zhang, H.-M.; Zhao, W.; Xie, Z.-X.; Long, L.-S.; Mao, B.-W.; Xu, X.; Zheng, L.-S., One Step Fabrication of Metal-Organic Coordination Monolayers on Au(111) Surfaces. *Journal of Physical Chemistry C* **2007**, *111*, 7570-7573.

31. Liu, J.; Gao, Y.; Wang, T.; Xue, Q.; Hua, M.; Wang, Y.; Huang, L.; Lin, N., Collective Spin Manipulation in Antiferroelastic Spin-Crossover Metallo-Supramolecular Chains. *ACS Nano* **2020**, *14*, 11283-11293.

32. Hohenberg, P.; Kohn, W., Inhomogeneous Electron Gas. *Physical Review B* **1964**, *136*, B864.

33. Kohn, W.; Sham, L. J., Self-Consistent Equations Including Exchange and Correlation Effects. *Physical Review* **1965**, *140*, A1133.

34. Meir, Y.; Wingreen, N. S., Landauer Formula for the Current through an Interacting Electron Region. *Physical Review Letters* **1992**, *68*, 2512-2515.

35. Y. Q. Xue, S. Datta, M. A. Ratner, Chem. Phys. 2002, 281, 151-170.

36. M. Brandbyge, J. L. Mozos, P. Ordejon, J. Taylor, K. Stokbro, Phys. Rev. B 2002, 65, 165401

37. J. X. Zhang, S. M. Hou, R. Li, Z. K. Qian, R. S. Han, Z. Y. Shen, X. Y. Zhao, Z. Q. Xue, Nanotechnology 2005, 16, 3057-3063.

38. R. Li, J. Zhang, S. Hou, Z. Qian, Z. Shen, X. Zhao, Z. Xue, Chem. Phys. 2007, 336, 127-135.

39. Soler, J. M.; Artacho, E.; Gale, J. D.; Garcia, A.; Junquera, J.; Ordejon, P.; Sanchez-Portal, D., The Siesta Method for Ab Initio Order-N Materials Simulation. *Journal of Physics-Condensed Matter* **2002**, *14*, 2745-2779.

40. Garcia, A., et al., Siesta: Recent Developments and Applications. *Journal of Chemical Physics* **2020**, *152*, 204108.

41. Perdew, J. P.; Burke, K.; Ernzerhof, M., Generalized Gradient Approximation Made Simple. *Physical Review Letters* **1996**, *77*, 3865-3868.

42. Troullier, N.; Martins, J. L., Efficient Pseudopotentials for Plane-Wave Calculations. *Physical Review B* **1991**, *43*, 1993-2006.

43. Rivero, P.; Manuel Garcia-Suarez, V.; Pereniguez, D.; Utt, K.; Yang, Y.; Bellaiche, L.; Park, K.; Ferrer, J.; Barraza-Lopez, S., Systematic Pseudopotentials from Reference Eigenvalue Sets for Dft Calculations. *Computational Materials Science* **2015**, *98*, 372-389.

44. Kresse, G.; Joubert, D., From Ultrasoft Pseudopotentials to the Projector Augmented-Wave Method. *Physical Review B* **1999**, *59*, 1758-1775.

45. Rocha, A. R.; Garcia-Suarez, V. M.; Bailey, S. W.; Lambert, C. J.; Ferrer, J.; Sanvito, S., Towards Molecular Spintronics. *Nature Materials* **2005**, *4*, 335-339.

46. Rocha, A. R.; Garcia-Suarez, V. M.; Bailey, S.; Lambert, C.; Ferrer, J.; Sanvito, S., Spin and Molecular Electronics in Atomically Generated Orbital Landscapes. *Physical Review B* **2006**, *73*, 085414.

47. Rungger, I.; Sanvito, S., Algorithm for the Construction of Self-Energies for Electronic Transport Calculations Based on Singularity Elimination and Singular Value Decomposition. *Physical Review B* **2008**, *78*, 035407.

48. Li, R.; Hou, S.; Zhang, J.; Qian, Z.; Shen, Z.; Zhao, X., Analysis on the Contribution of Molecular Orbitals to the Conductance of Molecular Electronic Devices. *Journal of Chemical Physics* **2006**, *125*, 194113.

49. Paulsson, M.; Brandbyge, M., Transmission Eigenchannels from Nonequilibrium Green's Functions. *Physical Review B* **2007**, *76*, 115117.

50. Billas, I. M. L.; Chatelain, A.; Deheer, W. A., Magnetism from the Atom to the Bulk in Iron, Cobalt, and Nickel Clusters. *Science* 1994, 265, 1682-1684.

51. Mittendorfer, F.; Eichler, A.; Hafner, J., Structural, Electronic and Magnetic Properties of Nickel Surfaces. *Surface Science* 1999, 423, 1-11.

52. Roth, W. L., Magnetic Structures of MnO, FeO, CoO, and NiO. *Physical Review* 1958, 110, 1333-1341.

53. Nitzan, A., Electron Transmission through Molecules and Molecular Interfaces. *Annual Review of Physical Chemistry* **2001**, *52*, 681-750.

54. Prasongkit, J.; Rocha, A. R., Quantum Interference Effects in Biphenyl Dithiol for Gas Detection. *RSC Advances* **2016**, *6*, 59299-59304.

55. Zou, D.; Zhao, W.; Cui, B.; Li, D.; Liu, D., Adsorption of Gas Molecules on a Manganese Phthalocyanine Molecular Device and Its Possibility as a Gas Sensor. *Physical Chemistry Chemical Physics* **2018**, *20*, 2048-2056.

56. Noori, M., et al., Tuning the Electrical Conductance of Metalloporphyrin Supramolecular Wires. *Scientific Reports* **2016**, *6,* 37352.

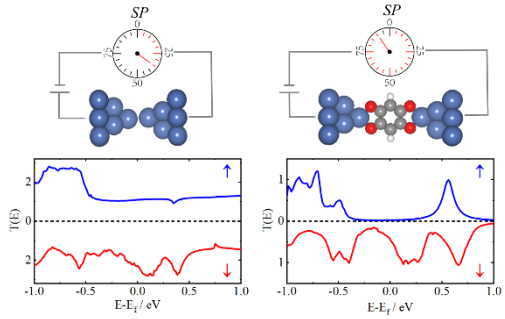


**Abstract Graphics**